A Generic Space-Time-Frequency Correlation Model and Its Corresponding Simulation Model for Narrowband MIMO Channels

Xiang Cheng*, Cheng-Xiang Wang*, and David I. Laurenson†

*Joint Research Institute in Signal and Image Processing,
School of Engineering & Physical Sciences, Heriot-Watt University, Edinburgh, EH14 4AS, U.K.
E-mail: {xc48, cheng-xiang.wang}@hw.ac.uk
†Joint Research Institute in Signal and Image Processing,
School of Engineering and Electronics, University of Edinburgh, Edinburgh, EH9 3JL, U.K.
E-mail: Dave.Laurenson@ed.ac.uk

Keyword: Wireless channels, MIMO, STF correlation, deterministic simulation model.

Abstract

For the analysis and design of Multiple-Input Multiple-Output (MIMO) wireless communication systems with frequency diversity features, e.g., MIMO-Orthogonal Frequency Division Multiplexing (MIMO-OFDM) systems, it is often desirable to develop a channel model that can characterise the three-dimensional (3-D) space-time-frequency (STF) correlation properties over the links of the underlying MIMO channels. In this paper, we propose a generic 3-D STF correlation model, which includes many well-known existing models as special cases, with closed-form expressions of the STF correlation properties. Based on the developed theoretical reference model, a deterministic simulation model is then proposed and its 3-D STF correlation properties are also investigated by providing closed-form expressions. It is shown that the correlation properties of the simulation model fit those of the reference model very well when the parameters of the simulation model are determined by using the L*p*-norm method (LPNM).

1 Introduction

MIMO systems have recently received much attention because of their potential for achieving higher data rate and providing more reliable reception performance compared with traditional single-antenna systems for wireless communications. In order to theoretically analyse and design high performance MIMO wireless systems under various circumstances, it is of great importance to have proper theoretical reference models [20] for the underlying MIMO wireless channels. Furthermore, for the practical simulation and performance evaluation of MIMO systems, it is advantageous to develop accurate MIMO channel simulation models [14]. Nowadays, 3-D STF correlation models are required to comprehensively understand the behaviour of MIMO wireless channels with frequency diversity features, e.g., in MIMO-OFDM systems [4].

Most existing models, e.g., [1,2,6,14], were proposed to investigate 2-D space-time (ST) correlation properties of narrowband MIMO wireless channels, but the frequency correlation properties of two sub-channels in a MIMO channel were not well understood. In [19], only 2-D time-frequency (TF) correlation reference and simulation models were studied for frequency correlated single-input single-output (SISO) channels under isotropic scattering assumptions. The authors in [13] investigated space, time, and frequency correlation properties separately of MIMO channels based on the elliptical geometry of scatterers for microcellular environments. However, in [13], no one generic STF correlation function (CF) was given. Moreover, the integral expressions of the derived space and time CFs can only be numerically evaluated as no closed-form expressions were found. Rad and Gazor proposed non-geometric 3-D STF correlation models for MIMO outdoor channels [8,15,16], where the angle of arrival (AoA) and angle of departure (AoD) were assumed to be independent.

In this paper, we first derive a generic theoretical reference model in order to study the 3-D STF correlation properties between the impulse responses of two sub-channels with different carrier frequencies in a narrowband MIMO channel. Different from [13], the proposed reference model is based on the well-known geometrical one-ring scattering model [1,6], which has widely been used for modelling MIMO channels in macrocelluar environments due to its simplicity, and has a closed-form expression of the generic STF CF. In contrast to non-geometric models [8,15,16], the proposed model characterises the AoA using the von Mises angular probability density function (PDF) [2], which is applicable to both isotropic and non-isotropic scattering environments, and considers the interdependence between the AoA and AoD. More importantly, we will demonstrate that the derived generic closed-form expression is valid not only for the 3-D STF CF, but also its degenerate 2-D and 1-D CFs, e.g., ST CF and frequency CF. This means that all the CFs have a uniform expression but with different parameters. The derived new 3-D STF correlation model is a generalization of many existing models [1,2,6,7,10,11].

Due to its infinite complexity, the proposed narrowband one-ring STF MIMO reference model cannot be realized directly in software or hardware. Therefore, the corresponding simulation model is very important in practice for the performance evaluation of MIMO wireless communication systems. The second part of this paper uses the reference model as the starting point for the derivation of an efficient simulation model by taking into account all the 3-D STF correlation properties of MIMO channels. The proposed procedure is based on the principle of deterministic channel modelling [12]. Closed-form expressions will be provided for all the 3-D, 2-D, and 1-D CFs of the simulation model. This allows us to assess the performance of the simulation model analytically by comparing its correlation properties with those of the developed generic reference model. It is shown that the designed MIMO channel simulator matches the underlying reference model very well with respect to temporal, spatial, and frequency properties.

The paper is structured as follows. The one-ring narrowband MIMO channel model is introduced in Section 2 and the new generic closed-form 3-D STF CF is derived in Section 3. In Section 4, an efficient deterministic simulation model is proposed and its corresponding 3-D STF CF is derived as a closed-form expression. Some simulation results are presented and the performance of the resulting simulation model is evaluated in Section 5. Finally, conclusions are drawn in Section 6.

2 The one-ring narrowband MIMO model

A one-ring narrowband MIMO channel model was first proposed in [6] and further developed in [1]. The one-ring model is appropriate for describing scattering environments where the transmitter base station (BS) is elevated and unobstructed, whereas the receiver mobile station (MS) is surrounded by a large number of local scatterers. Each scatterer is assumed to be reflected only once. Let us consider a one-ring narrowband MIMO channel model shown in Fig. 1. The BS and MS have n_{BS} and n_{MS} omni-directional antenna elements in the horizontal plane, respectively. Without loss of generality, we consider uniform linear antenna arrays with $n_{BS} = n_{MS} = 2$ (a 2×2 MIMO channel). The antenna element spacings at the BS and MS are designated by δ_T and δ_R, respectively. The local scatterers are located on a ring surrounding the MS with radius R. It is usually assumed that R is much smaller than D, denoting the distance between the BS and MS. Furthermore, it is assumed that both R and D are much larger than the antenna element spacings δ_T and δ_R, i.e., $D >> R >> \max\{\delta_T, \delta_R\}$. The multi-element antenna tilt angles are denoted by α and β. The MS moves with a speed v in the direction determined by the angle of motion γ. The angle spread seen at the BS is denoted by Δ, which is related to R and D by $\Delta \approx \arctan(R/D) \approx R/D$.

Without a line-of-sight component, the sub-channel complex impulse responses at two different carrier frequencies f_c and $f_c^\dagger$ can be expressed as:

$$h_{lp}(t) = h_{1,lp}(t) + jh_{2,lp}(t) = \lim_{N\to\infty}\frac{1}{\sqrt{N}}\sum_{n=1}^{N}\exp\{j[\psi_n - 2\pi f_c\tau_{lp,n} + 2\pi f_D t\cos(\phi_n^R - \gamma)]\}, \tag{1a}$$

$$h_{mq}^\dagger(t) = h_{1,mq}^\dagger(t) + jh_{2,mq}^\dagger(t) = \lim_{N\to\infty}\frac{1}{\sqrt{N}}\sum_{n=1}^{N}\exp\{j[\psi_n - 2\pi f_c^\dagger\tau_{mq,n} + 2\pi f_D t\cos(\phi_n^R - \gamma)]\}, \tag{1b}$$

with $l, m = 1,2,\ldots,n_{MS}$, $p, q = 1,2,\ldots,n_{BS}$, $\tau_{lp,n} = (\xi_{pn} + \xi_{nl})/c$, and $\tau_{mq,n} = (\xi_{qn} + \xi_{nm})/c$, where $\tau_{lp,n}$ ($\tau_{mq,n}$) is the travel time of the wave through the link $T_p - S_n - R_l$ ($T_q - S_n - R_m$) scattered by the nth scatterer, S_n, and c is the speed of light. The AoA of the wave travelling from the nth scatterer towards the MS is denoted by ϕ_n^R, while ξ_{pn}, ξ_{nl}, ξ_{qn}, and ξ_{nm} are the distances as functions of ϕ_n^R as shown in Fig. 1. According to [1], we have the following approximate equations

$$\xi_{pn} \approx \zeta_n - \frac{\delta_T}{2}[\cos(\alpha) + \Delta\sin(\alpha)\sin(\phi_n^R)], \tag{2a}$$

$$\xi_{qn} \approx \zeta_n + \frac{\delta_T}{2}[\cos(\alpha) + \Delta\sin(\alpha)\sin(\phi_n^R)], \tag{2b}$$

$$\xi_{nl} \approx R - \frac{\delta_R}{2}\cos(\phi_n^R - \beta), \tag{2c}$$

$$\xi_{nm} \approx R + \frac{\delta_R}{2}\cos(\phi_n^R - \beta), \tag{2d}$$

$$\zeta_n \approx D + R\cos(\phi_n^R). \tag{2e}$$

The phases ψ_n are independent and identically distributed (i.i.d.) random variables with uniform distributions over $[0,2\pi)$; f_D is the maximum Doppler frequency; $h_{1,lp}(t)$ ($h_{1,mq}^\dagger(t)$) and $h_{2,lp}(t)$ ($h_{2,mq}^\dagger(t)$) are the inphase and quadrature components of the complex impulse response $h_{lp}(t)$ ($h_{mq}^\dagger(t)$), respectively; and N is the number of independent scatterers, S_n, around the MS.

In the literature, many different scatterer distributions have been proposed to characterise the AoA, ϕ_n^R, such as the uniform [17], Gaussian [3], wrapped Gaussian [18], and the cardioid PDFs [5]. In this paper, the von Mises PDF [2] is used, which can approximate all the above mentioned distributions. In [2], it was shown that this PDF fits the real data very well. The von Mises PDF is defined as [2]

$$f(\phi^R) = \frac{\exp[k\cos(\phi^R - \mu)]}{2\pi I_0(k)}, \qquad \phi^R \in [0,2\pi), \tag{3}$$

where ϕ^R is the continuous denotation of ϕ_n^R when N is infinite, $I_0(\cdot)$ is the zeroth-order modified Bessel function of the first kind, $\mu \in [0,2\pi)$ accounts for the mean value of the AoA, ϕ^R, and k ($k \geq 0$) is a real-valued parameter that controls the angular spread of the AOA ϕ^R. For $k = 0$ (isotropic scattering), the von Mises PDF reduces to the uniform distribution, while for $k>0$ (non-isotropic scattering), the von Mises PDF approximates different distributions depending on different values of k [2].

3 The new generic STF CF

From (1), it follows that the correlation properties of $h_{lp}(t)$ and $h_{mq}^\dagger(t)$ are completely determined by the underlying real Gaussian noise processes $h_{u,lp}(t)$ and $h_{v,mq}^\dagger(t)$ ($u, v = 1,2$). Therefore, we can restrict our investigations to the following STF CF

$$\rho_{h_{u,lp}h_{v,mq}^\dagger}(\tau,\chi) := E[h_{u,lp}(t)h_{v,mq}^\dagger(t+\tau)], \tag{4}$$

where $E[\cdot]$ denotes the statistical average with respect to ϕ_n^R and ψ_n. It should be observed that (4) is a function of the time separation, τ, space separation, δ_T and δ_R, and frequency separation, $\chi = f_c^\dagger - f_c$.

Substituting (1)–(3) into (4) and after some mathematical manipulations, the 3-D STF CFs between $h_{u,lp}(t)$ and $h_{u,mq}^\dagger(t+\tau)$, and similarly between $h_{u,lp}(t)$ and $h_{v,mq}^\dagger(t+\tau)$, are given by

$$\rho_{h_{1,lp}h_{1,mq}^\dagger}(\tau,\chi) = \rho_{h_{2,lp}h_{2,mq}^\dagger}(\tau,\chi) = \frac{1}{4I_0(k)}\left\{e^{jC}I_0\left[(A-jB)^{1/2}\right] + e^{-jC}I_0\left[(A+jB)^{1/2}\right]\right\}, \tag{5a}$$

$$\rho_{h_{1,lp}h_{2,mq}^\dagger}(\tau,\chi) = -\rho_{h_{2,lp}h_{1,mq}^\dagger}(\tau,\chi) = \frac{1}{4jI_0(k)}\left\{e^{-jC}I_0\left[(A+jB)^{1/2}\right] - e^{jC}I_0\left[(A-jB)^{1/2}\right]\right\}, \tag{5b}$$

respectively. Since the derivations of (5a) and (5b) are similar, only the derivation of (5a) is given in the Appendix. Consequently, the 3-D STF CF between the complex impulse responses $h_{lp}(t)$ and $h_{mq}^\dagger(t)$ can be directly obtained as

$$\rho_{h_{lp}h_{mq}^\dagger}(\tau,\chi) = 2\rho_{h_{1,lp}h_{1,mq}^\dagger}(\tau,\chi) - j2\rho_{h_{1,lp}h_{2,mq}^\dagger}(\tau,\chi) = \frac{1}{I_0(k)}e^{jC}I_0\left[(A-jB)^{1/2}\right] \tag{6}$$

where

$$A = k^2 - x^2 - y^2 - z^2\Delta^2\sin^2\alpha - 2yz\Delta\sin\alpha\sin\beta + 2xy\cos(\beta-\gamma) + 2xz\Delta\sin\alpha\sin\gamma - X^2 J + 2xXK - 2yXL - 2zXM, \tag{7a}$$

$$B = 2k[x\cos(\gamma-\mu) - y\cos(\beta-\mu) - z\Delta\sin\alpha\sin\mu - XS], \tag{7b}$$

$$C = z\cos\alpha + XT, \tag{7c}$$

with

$$x = 2\pi f_D\tau, \tag{8a}$$

$$y = 2\pi f_c\delta_R/c, \tag{8b}$$

$$z = 2\pi f_c\delta_T/c, \tag{8c}$$

$$X = 2\pi\chi/c, \tag{8d}$$

$$J = R^2 + (\delta_T^2/4)\Delta^2\sin^2\alpha + \delta_R^2/4 + R\delta_R\cos\beta + (\delta_T\delta_R/2)\Delta\sin\alpha\sin\beta, \tag{8e}$$

$$K = R\cos\gamma + (\delta_T/2)\Delta\sin\alpha\sin\gamma + (\delta_R/2)\cos(\beta-\gamma), \tag{8f}$$

$$L = R\cos\beta + (\delta_T/2)\Delta\sin\alpha\sin\beta + (\delta_R/2), \tag{8g}$$

$$M = (\delta_T/2)\Delta^2\sin^2\alpha + (\delta_R/2)\Delta\sin\alpha\sin\beta, \tag{8h}$$

$$S = R\cos\mu + (\delta_T/2)\Delta\sin\alpha\sin\mu + (\delta_R/2)\cos(\beta-\mu), \tag{8i}$$

$$T = (\delta_T/2)\cos\alpha + D + R. \tag{8j}$$

It is worth stressing here that (5) and (6) are the generic expressions which apply to the 3-D STF CF and the subsequently presented 2-D and 1-D CFs differ only in values of *A*, *B*, and *C*. The corresponding expressions of *A*, *B*, and *C* for the degenerate 2-D and 1-D CFs can be easily obtained from (7) by setting relevant terms to zero. For example, setting the frequency separation $\chi = 0$ (X=0) in (7) gives the following expressions of *A*, *B*, and *C* for the 2-D ST CF:

$$A = k^2 - x^2 - y^2 - z^2\Delta^2\sin^2\alpha - 2yz\Delta\sin\alpha\sin\beta + 2xy\cos(\beta-\gamma) + 2xz\Delta\sin\alpha\sin\gamma, \tag{9a}$$

$$B = 2k[x\cos(\gamma-\mu) - y\cos(\beta-\mu) - z\Delta\sin\alpha\sin\mu], \tag{9b}$$

$$C = z\cos\alpha. \tag{9c}$$

From (5b), we find that the STF CF $\rho_{h_{1,lp}h_{2,mq}^\dagger}(\tau,\chi) = -\rho_{h_{2,lp}h_{1,mq}^\dagger}(\tau,\chi) = 0$ if $B=0$ and $C=0$. From (7b), it is clear that $B=0$ if $k=0$ holds. This means that $B=0$ in isotropic scattering environments. By setting the space separation at the BS $\delta_T = 0$ (z=0) and the frequency separation $\chi = 0$ (X=0) in (7c), we can get C=0 for the 2-D ST CF (single-input multiple-output (SIMO) case) and 1-D time CF. This clearly indicates that the 2-D ST CF $\rho_{h_{1,lp}h_{2,lq}}(\tau) = -\rho_{h_{2,lp}h_{1,lq}}(\tau) = 0$ (SIMO case) and 1-D time CF $\rho_{h_{1,lp}h_{2,lp}}(\tau) = -\rho_{h_{2,lp}h_{1,lp}}(\tau) = 0$ in isotropic scattering environments. When setting the frequency separation χ=0 (X=0) and the tilt angle of the BS $\alpha=\pi/2$ in (7c), we can also obtain $C=0$ for the 2-D ST CF (MIMO case), 1-D space CF, and 1-D time CF. This means that in isotropic scattering environments, the 2-D ST CF $\rho_{h_{1,lp}h_{2,mq}}(\tau) = -\rho_{h_{2,lp}h_{1,mq}}(\tau) = 0$ (MIMO case), 1-D space CF $\rho_{h_{1,lp}h_{2,mq}} = -\rho_{h_{2,lp}h_{1,mq}} = 0$, and 1-D time CF $\rho_{h_{1,lp}h_{2,lp}}(\tau) = -\rho_{h_{2,lp}h_{1,lp}}(\tau) = 0$.

The proposed generic 3-D STF correlation model with a closed-form expression (6) includes many existing models as special cases. For a SISO case, the time CF given in [2] is obtained by setting $\delta_T = \delta_R = 0$ and $\chi = 0$ in (6) with $k \neq 0$. If by further setting $k=0$ (isotropic scattering) in (6), the Clarke's time CF in [10] is obtained. For a SIMO case, the Lee's ST CF in [11] is obtained by substituting $\delta_T = 0$, $\chi = 0$, $\beta = \pi$, and $k=0$ into (6). For a multiple-input single-output (MISO) case, the ST CF in [6] is obtained by substituting $\delta_R = 0$, $\chi = 0$, and $k=0$ into (6). If further substituting $f_D = 0$ into (6), the space CF given in [7] is obtained. For a MIMO case, the ST CF shown in [1] is obtained by setting $\chi = 0$ in (6) with $k \neq 0$.

4 The deterministic simulation model

In this section, an efficient deterministic simulation model is proposed, which is obtained from the reference model by utilizing only a finite number of scatterers, *N*, and keeping all the model parameters fixed. Hence, the impulse responses $\tilde{h}_{lp}(t)$ and $\tilde{h}_{mq}^\dagger(t)$ of the deterministic simulation model are modelled as

$$\tilde{h}_{lp}(t) = \tilde{h}_{1,lp}(t) + j\tilde{h}_{2,lp}(t) = \frac{1}{\sqrt{N}}\sum_{n=1}^{N}\exp\left\{j\left[\tilde{\psi}_n - 2\pi f_c\tau_{lp,n} + 2\pi f_D t\cos\left(\tilde{\phi}_n^R - \gamma\right)\right]\right\}, \tag{10a}$$

$$\tilde{h}_{mq}^\dagger(t) = \tilde{h}_{1,mq}^\dagger(t) + j\tilde{h}_{2,mq}^\dagger(t) = \frac{1}{\sqrt{N}}\sum_{n=1}^{N}\exp\left\{j\left[\tilde{\psi}_n - 2\pi f_c^\dagger\tau_{mq,n} + 2\pi f_D t\cos\left(\tilde{\phi}_n^R - \gamma\right)\right]\right\}, \tag{10b}$$

where the phases $\tilde{\psi}_n$ are simply the outcomes of a random generator uniformly distributed over $[0,2\pi)$, the discrete AoAs $\tilde{\phi}_n^R$ will be kept constant during simulation, and the other symbol definitions are the same as in (1). Therefore, we can analyse the properties of the deterministic channel simulator by time averages instead of statistical averages. Similar to (4), the 3-D STF CF can be defined as

$$\tilde{\rho}_{h_{u,lp}h^{\dagger}_{v,mq}}(\tau,\chi) := \left\langle \tilde{h}_{u,lp}(t)\tilde{h}^{\dagger}_{v,mq}(t+\tau)\right\rangle, \tag{11}$$

where $\langle\cdot\rangle$ denotes the time average operator. Substituting (10) into (11), it is shown that (11) can be expressed in the closed-form as

$$\begin{aligned}\tilde{\rho}_{h_{1,lp}h^{\dagger}_{1,mq}}(\tau,\chi) &= \tilde{\rho}_{h_{2,lp}h^{\dagger}_{2,mq}}(\tau,\chi)\\ &= \frac{1}{2N}\sum_{n=1}^{N}\Big[\cos(C)\cos\left(P\cos\tilde{\phi}_n^R + Q\sin\tilde{\phi}_n^R\right) \\ &\quad -\sin(C)\sin\left(P\cos\tilde{\phi}_n^R + Q\sin\tilde{\phi}_n^R\right)\Big],\end{aligned} \tag{12a}$$

$$\begin{aligned}\tilde{\rho}_{h_{1,lp}h^{\dagger}_{2,mq}}(\tau,\chi) &= -\tilde{\rho}_{h_{2,lp}h^{\dagger}_{1,mq}}(\tau,\chi)\\ &= -\frac{1}{2N}\sum_{n=1}^{N}\Big[\sin(C)\cos\left(P\cos\tilde{\phi}_n^R + Q\sin\tilde{\phi}_n^R\right) \\ &\quad +\cos(C)\sin\left(P\cos\tilde{\phi}_n^R + Q\sin\tilde{\phi}_n^R\right)\Big].\end{aligned} \tag{12b}$$

By analogy with (6), we can further get the 3-D STF CF between $\tilde{h}_{lp}(t)$ and $\tilde{h}^{\dagger}_{mq}(t)$ as

$$\begin{aligned}\tilde{\rho}_{h_{lp}h^{\dagger}_{mq}}(\tau,\chi) &= 2\tilde{\rho}_{h_{1,lp}h^{\dagger}_{1,mq}}(\tau,\chi) - j2\tilde{\rho}_{h_{1,lp}h^{\dagger}_{2,mq}}(\tau,\chi)\\ &= \frac{1}{N}\sum_{n=1}^{N} e^{jC} e^{j\left(P\cos\tilde{\phi}_n^R + Q\sin\tilde{\phi}_n^R\right)},\end{aligned} \tag{13}$$

where C is the same as in (6), while

$$P = XY + y\cos\beta - x\cos\gamma, \tag{14a}$$

$$Q = XZ + y\sin\beta + z\Delta\sin\alpha - x\sin\gamma, \tag{14b}$$

with

$$Y = R + (\delta_R/2)\cos\beta \tag{15a}$$

$$Z = (\delta_T/2)\Delta\sin\alpha + (\delta_R/2)\sin\beta. \tag{15b}$$

Note that x, y, z, and X are the same as defined in (8a)–(8d) above. Similarly to (5) and (6), (12) and (13) are the generic expressions which apply to all the 3-D, 2-D, and 1-D CFs of the deterministic simulation model with different C, P, and Q. The corresponding expressions of P and Q for the degenerate 2-D and 1-D CFs can easily be obtained from (14) by setting some relevant terms to zero. Comparing (14) with (7), we can relate A and B to P and Q by

$$A = a^2 + b^2 - \left(P^2 + Q^2\right), \tag{16a}$$

$$B = -2(aP + bQ). \tag{16b}$$

From (12) and (13), it is obvious that only $\{\phi_n^R\}_{n=1}^{N}$ needs to be determined for this deterministic simulation model.

4.1 Parameter computation method

In this subsection, we will apply the LPNM [12] to compute the model parameters $\{\phi_n^R\}_{n=1}^{N}$ of the deterministic simulation model based on corresponding properties of the reference model. The 1-D time CF $\rho_{h_{lp}h_{lq}}(\tau)$, 1-D frequency CF $\rho_{h_{lp}h^{\dagger}_{lp}}(\chi)$ and 2-D space CF $\rho_{h_{lp}h_{mq}}$ are identified as key properties. Then the LPNM requires the numerical minimization of the following three L_p-norms:

$$E_1^{(p)} := \left\{\frac{1}{\tau_{\max}}\int_0^{\tau_{\max}}\left|\rho_{h_{lp}h_{lp}}(\tau) - \tilde{\rho}_{h_{lp}h_{lp}}(\tau)\right|^p d\tau\right\}^{1/p}, \tag{17a}$$

$$E_2^{(p)} := \left\{\frac{1}{\chi_{\max}}\int_0^{\chi_{\max}}\left|\rho_{h_{lp}h^{\dagger}_{lp}}(\chi) - \tilde{\rho}_{h_{lp}h^{\dagger}_{lp}}(\chi)\right|^p d\chi\right\}^{1/p}, \tag{17b}$$

$$E_3^{(p)} := \left\{\frac{1}{\delta_T^{\max}\delta_R^{\max}}\int_0^{\delta_T^{\max}}\int_0^{\delta_R^{\max}}\left|\rho_{h_{lp}h_{mq}} - \tilde{\rho}_{h_{lp}h_{mq}}\right|^p d\delta_T d\delta_R\right\}^{1/p}, \tag{17c}$$

where $p = 1,2,\ldots$ Note that $\tau_{\max}$, $\chi_{\max}$, and $\delta_T^{\max}$ and $\delta_R^{\max}$ define the upper limits of the ranges over which the approximations $\tilde{\rho}_{h_{lp}h_{lp}}(\tau) \approx \rho_{h_{lp}h_{lp}}(\tau)$, $\tilde{\rho}_{h_{lp}h^{\dagger}_{lp}}(\chi) \approx \rho_{h_{lp}h^{\dagger}_{lp}}(\chi)$, and $\tilde{\rho}_{h_{lp}h_{mq}} \approx \rho_{h_{lp}h_{mq}}$ are of interest. For $\tilde{\rho}_{h_{lp}h^{\dagger}_{lp}}(\chi)$ and $\tilde{\rho}_{h_{lp}h_{mq}}$, if we replace ϕ_n^R by $\phi_n'^R$ and $\phi_n''^R$, respectively, the three error norms $E_1^{(p)}$, $E_2^{(p)}$, and $E_3^{(p)}$ can be minimized independently.

5 Simulation results

In this section, due to the limitation of space, we will only focus on the frequency correlation properties based on (6), and will evaluate the performance of the simulation model. The basic parameters are as follows: f_c=1 GHz, f_D=93 Hz, $c = 3\times10^8$ m/s, $D = 1200$ m, $R = 100$ m, $k = 3$, $\mu = \pi$, $\alpha = \pi/6$, $\beta = \pi/3$, and $\gamma = 7\pi/12$.

Figs. 2 and 3 illustrate the 2-D space-frequency (SF) CFs against the frequency separation and space separation at the BS and MS, respectively. Comparing them, we find that the influence of the normalized antenna space at the MS is greater than at the BS, since the angular spread, Δ, at the BS is generally small for the macrocellular case. Fig. 4 shows the 2-D TF CF along with the frequency separation and time separation. As shown in Figs. 2–4, the 2-D CFs take the maximum values when the frequency separation χ =0 and decrease with the increase of the frequency separation. Figs. 2–4 reveal that the shapes of CFs depend on time separation, frequency separation, and antenna spacing. Comparing (a) with (b) in Figs. 2–4, it is obvious that the normalized antenna space at the MS or BS has a large effect on the 2-D SF CFs, while its influence on the 2-D TF CF is negligibly small.

A plot of the function $\rho_{h_{lp}h_{lp}}(\tau)$ of the reference model is shown in Fig. 5. This figure also shows the resulting 1-D time CF $\tilde{\rho}_{h_{lp}h_{lp}}(\tau)$ of the simulation model designed with the LPNM using $p = 2$, $N = 30$, and $\tau_{\max} = 0.08$ s. Fig. 6 depicts the 1-D frequency CF $\rho_{h_{lp}h^{\dagger}_{lp}}(\chi)$ of the reference model and $\tilde{\rho}_{h_{lp}h^{\dagger}_{lp}}(\chi)$ of the simulation model, when applying the LPNM with $p = 2$, $N = 30$, and $\chi_{\max} = 8$ MHz. Fig. 7 depicts the 2-D space CF $\rho_{h_{lp}h_{mq}}$ of the reference model and $\tilde{\rho}_{h_{lp}h_{mq}}$ of the simulation model, with $N = 30$. The discrete AoAs $\phi_n''^R$ have been obtained by applying the LPNM on the error norm $E_3^{(p)}$ in (17c) with $p = 2$, $\delta_T^{\max} = 30\lambda$, and $\delta_R^{\max} = 3\lambda$. Figs. 5–7 clearly demonstrate that the proposed deterministic simulation model can fit the underlying reference model very well in terms of time, frequency, and space correlation properties.

6 Conclusions

In this paper, based on the well-known narrowband one-ring MIMO channel model, we have proposed a novel generic 3-D STF correlation reference model. The developed reference model is suitable for the analysis and design of MIMO wireless communication systems with frequency diversity features, e.g., MIMO-OFDM systems. The proposed 3-D STF reference model is general enough to include many well-known existing models as special cases. Depending on the developed theoretical reference model, a deterministic simulation model is then proposed. The corresponding 3-D STF CFs of the simulation model are derived with the closed-form expressions. Numerical results show that the correlation properties of the simulation model match those of the underlying theoretical model very closely.

Appendix

Derivation of (5a):

In this appendix, we derive the 3-D STF CF $\rho_{h_{1,lp}h^{\dagger}_{1,mq}}(\tau,\chi)$ of $h_{1,lp}(t)$ and $h^{\dagger}_{1,mq}(t+\tau)$ according to (4):

$$\begin{aligned}
&\rho_{h_{1,lp}h^{\dagger}_{1,mq}}(\tau,\chi)=E\left[h_{1,lp}(t)h^{\dagger}_{1,mq}(t+\tau)\right]\\
&=\lim_{N\to\infty}\frac{1}{N}\sum_{n=1}^{N}E\left\{\cos\left[\psi_n-2\pi f_c\tau_{lp,n}+2\pi f_D\cos\left(\phi_n^R-\gamma\right)t\right]\right.\\
&\left.\times\cos\left[\psi_n-2\pi f_c^{\dagger}\tau_{mq,n}+2\pi f_D\cos\left(\phi_n^R-\gamma\right)(t+\tau)\right]\right\}\\
&=\lim_{N\to\infty}\frac{1}{2N}\sum_{n=1}^{N}\cos\left[-2\pi f_c\left(\tau_{mq,n}-\tau_{lp,n}\right)\right.\\
&\left.-2\pi\chi\tau_{mq,n}+2\pi f_D\cos\left(\phi_n^R-\gamma\right)\tau\right]\\
&=\frac{1}{2}\int_0^{2\pi}\cos\left[-2\pi f_c\left(\tau_{mq}-\tau_{lp}\right)-2\pi\chi\tau_{mq}\right.\\
&\left.+2\pi f_D\cos\left(\phi^R-\gamma\right)\tau\right]f\left(\phi^R\right)d\phi^R,
\end{aligned}\tag{18}$$

where $\tau_{lp}=\left(\xi_{p\phi^R}+\xi_{\phi R_l}\right)/c$, $\tau_{mq}=\left(\xi_{q\phi^R}+\xi_{\phi R_m}\right)/c$. The terms $\xi_{p\phi^R}$, $\xi_{p\phi^R}$, $\xi_{\phi^R_l}$, and $\xi_{\phi^R_m}$ are obtained by replacing ϕ_n^R by ϕ^R in (2). Substituting all the above mentioned terms and PDF into (18) and considering (14), we have

$$\begin{aligned}
\rho_{h_{1,lp}h^{\dagger}_{1,mq}}(\tau,\chi)=&\frac{1}{4\pi I_0(k)}\\
&\times\int_0^{2\pi}\exp\left[k\cos\mu\cos\phi^R+k\sin\mu\sin\phi^R\right]\\
&\times\cos\left[C+P\cos\phi^R+Q\sin\phi^R\right]d\phi^R.
\end{aligned}\tag{19}$$

The definite integral in the right hand side of the above equation can be solved by using [9, eq. 3.937-1, pp. 522]. After some manipulations and considering (16), the closed-form expression for the 3-D STF CF $\rho_{h_{1,lp}h^{\dagger}_{1,mq}}(\tau,\chi)$ is given by (5a).

References

[1] A. Abdi, and M. Kaveh, "A space-time correlation model for multielement antenna systems in mobile fading channels," *IEEE J. Select. Areas Commun.*, **volume 20**, no. 3, pp. 550-560, (2002).

[2] A. Abdi, J. A. Barger, and M. Kaveh, "A parametric model for the distribution of the angle of arrival and the associated correlation function and power spectrum at the mobile station," *IEEE Trans. Veh. Technol.*, **volume 51**, no. 3, pp. 425-434, (2002).

[3] F. Adachi, M. T. Feeney, A. G. Williamson, and J. D. Parsons, "Cross-correlation between the envelopes of 900 MHz signals received at a mobile radio base station site," *IEE Proc. F, Commun., Radar, Signal Processing*, **volume 133**, pp. 506-512, (1986).

[4] H. Bolcskei, M. Borgmann, and A. Paulraj, "Impact of the propagation environment on the performance of space-frequency code MIMO-OFDM," *IEEE Journal on Selected Areas in Commun.*, **volume 21**, no. 3, pp. 427-439, (2003).

[5] G. J. Byers, and F. Takawira, "Spatially and temporally correlated MIMO channels: modeling and capacity analysis," *IEEE Trans. Veh. Technol.*, **volume 53**, no. 3, pp. 634-643, (2004).

[6] T. A. Chen, M. P. Fitz, W. Y. Kuo, M. D. Zoltowski, and J. H. Grimm, "A space-time model for frequency nonselective Rayleigh fading channels with applications to space-time modems," *IEEE J. Select. Areas Commun.*, **volume 18**, pp. 1175-1190, (2000).

[7] T. Fulghum and K. Molnar, "The Jakes fading model incorporating angular spread for a disk of scatterers," *Proc. IEEE VTC*, Ottawa, ON, Canada, pp. 489-493, (1998).

[8] S. Gazor, and H. S. Rad, "Space-time-frequency characterization of MIMO wireless channels," *IEEE Trans. Wireless Commun.*, **volume 5**, no. 9, pp. 2369-2375, (2006).

[9] I. S. Gradshteyn, and I. M. Ryzhik, *Table of Integrals, Series, and Products*, 5th ed, A. Jeffrey, Ed. San Diego, CA: Academic, (1994).

[10] W. C. Jakes Ed., *Microwave Mobile Communications*, New Jersey: IEEE Press, (1994).

[11] W. C. L. Lee, "Level crossing rates of an equal-gain predetection diversity combiner," *IEEE Trans. Commun. Technol.*, **volume 18**, pp. 417-426, (1970).

[12] M. Pätzold, "Mobile Fading Channels", *Chichester: John Wiley & Sons*, (2002).

[13] M. Pätzold, and B. O. Hogstad, "A wideband MIMO channel model derived from the geometric elliptical scattering model," *Proc. ISWCS'06*, Valencia, Spain, pp. 138–143, (2006).

[14] M. Pätzold, and B. O. Hogstad, "A space-time channel simulator for MIMO channels based on the geometrical one-ring scattering model," *Wireless Communications on Mobile Computing*, **volume 4**, pp. 727–737, (2004).

[15] H. S. Rad, and S. Gazor, "Space-time-frequency characterization of 3d non-isotropic MIMO multicarrier propagation channels employing directional antennas,"

IEEE Trans. Wireless Commun., accepted with minor revision, (2007).

[16] H. S. Rad, and S. Gazor, "Space-time-frequency characterization of 3D non-isotropic MIMO multicarrier propagation channels employing directional antennas," *Proc. IEEE WCNC 2007*, Hong Kong, China, pp. 1890-1895, (2007).

[17] J. Salz, and J. H. Winters, "Effect of fading correlation on adaptive arrays in digital mobile radio," *IEEE Trans. Veh. Technol.*, **volume 43**, pp. 1049-1057, (1994).

[18] L. Schumacher, K. I. Pedersen, and P. E. Mogensen, "From antenna spacings to theoretical capacities - guidelines for simulating MIMO systems," *Proc. IEEE PIMRC*, **volume 2**, pp. 587-592, (2002).

[19] C. X. Wang, M. Pätzold, and Q. Yao, "Stochastic modelling and simulation of frequency correlated wideband fading channels," *IEEE Trans. Veh. Technol.*, **volume 56**, no. 3, pp. 1050-1063, (2007).

[20] K. Yu, "Multiple-input multiple-output radio propagation channels: characteristics and models," *doctoral thesis, Signals, Sensors and Systems, Royal Institute of Technology (KTH)*, (2005).

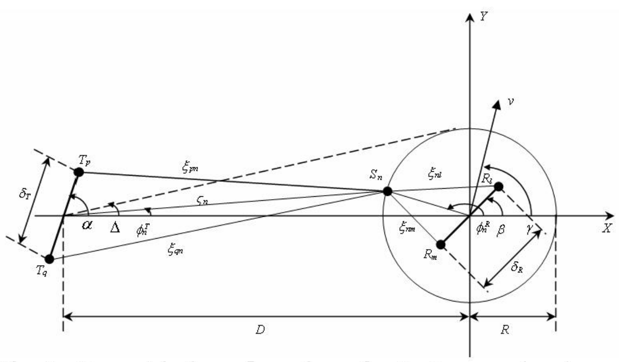

Fig. 1. Geometrical configuration of a 2×2 narrowband one-ring channel model with local scatters around the mobile user.

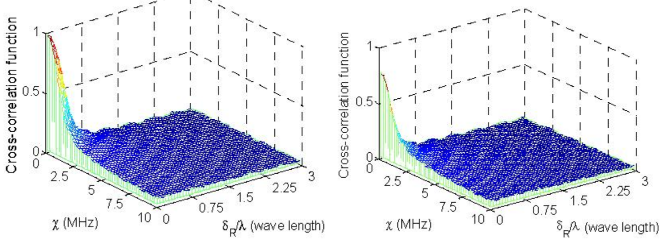

(a) (b)

Fig. 2. The 2-D SF CF $\rho_{h_{lp}h^{\dagger}_{mq}}(\chi)$ versus the frequency separation χ and the normalized antenna spacing at the MS δ_R/λ : (a) the normalized antenna spacing at the BS $\delta_T/\lambda=0$ (SIMO) and (b) the normalized antenna spacing at the BS $\delta_T/\lambda=5$ (MIMO).

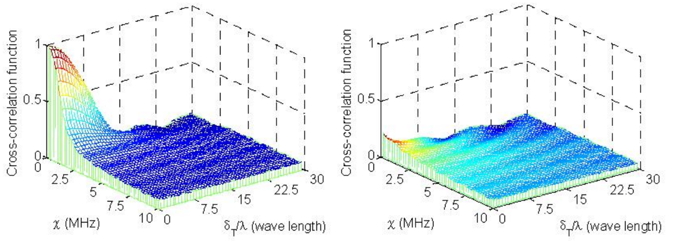

(a) (b)

Fig. 3. The 2-D SF CF $\rho_{h_{lp}h^{\dagger}_{mq}}(\chi)$ versus the frequency separation χ and the normalized antenna spacing at the BS δ_T/λ : (a) the normalized antenna spacing at the MS $\delta_R/\lambda=0$ (MISO) and (b) the normalized antenna spacing at the MS $\delta_R/\lambda=0.5$ (MIMO).

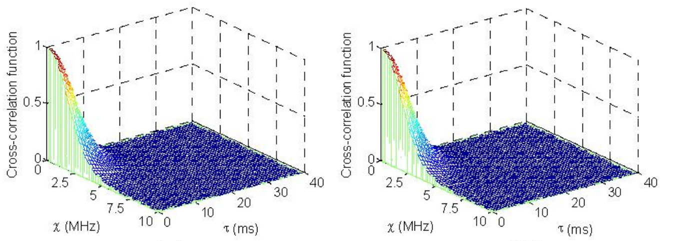

(a) (b)

Fig. 4. The 2-D TF CF $\rho_{h_{lp}h^{\dagger}_{lq}}(\tau,\chi)$ versus the time separation τ and frequency separation χ : (a) the normalized antenna spacing at the BS $\delta_T/\lambda=0$ and at the MS $\delta_R/\lambda=0$ (SISO) and (b) the normalized antenna spacing at the BS $\delta_T/\lambda=5$ and at the MS $\delta_R/\lambda=0.5$ (MIMO).

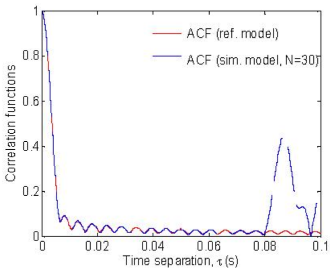

Fig. 5. The 1-D time CF $\rho_{h_{lp}h_{lp}}(\tau)$ (reference model) and $\tilde{\rho}_{h_{lp}h_{lp}}(\tau)$ (simulation model) with N=30.

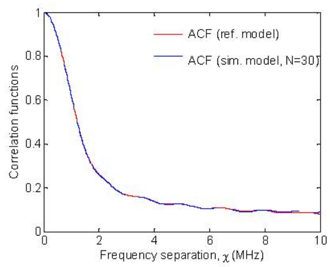

Fig. 6. The 1-D frequency CF $\rho_{h_{lp}h^{\dagger}_{lp}}(\chi)$ (reference model) and $\tilde{\rho}_{h_{lp}h^{\dagger}_{lp}}(\chi)$ (simulation model) with N=30.

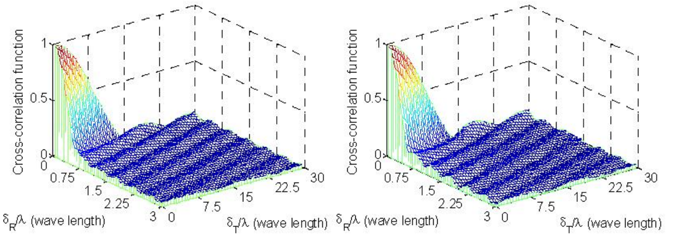

(a) (b)

Fig. 7. The 2-D space CF versus the normalized antenna spacing at the BS δ_T/λ and at the MS δ_R/λ : (a) $\rho_{h_{lp}h_{mq}}$ (reference model) and (b) $\tilde{\rho}_{h_{lp}h_{mq}}$ (simulation model) with N=30.